Fluid flow and heat transfer between finite rotating disks

Vijay K. Garg and A. Z. Szeri
Department of Mechanical Engineering, University of Pittsburgh, Pittsburgh, PA, USA

The laminar flow between finite rotating disks with a shroud has been analyzed using a velocity and a stream function formulation, employing Galerkin's method with B-spline basis. Though results from both formulations are in good agreement with the LDV data on velocity profiles, and with each other, we find the stream function formulation clearly superior computationally, and we employ it subsequently to study heat transfer between the disks. The calculations show strong boundary-layer character near the disks. The Nusselt number depends upon both geometry and the Reynolds number.

Keywords: fluid flow; heat transfer; finite rotating disks; cylindrical cavity

1. Introduction

The flow between rotating disks and the flow between rotating cylinders constitute two classes of swirling flows that have occupied a central position in the fluid mechanics research of this century. When the geometry of the flow domain is infinite in one dimension, leading to disks of infinite radius or to cylinders of infinite axial extent, the governing equations can be reduced to a system of ordinary differential equations. The solution of these equations was long thought to represent physical systems. However, it is now known that infinite geometry and finite geometry lead to qualitatively distinct behavior. For rotating cylinder flows, the infinite geometry provides for supercritical bifurcation of the Couette flow into Taylor vortex flow, but in a finite geometry the end effects are always felt irrespective of the aspect ratio (Benjamin, 1978; Dai and Szeri, 1990). For rotating disk flows, the infinite geometry supports a rich bifurcating structure. However, this does not seem to be the case for finite disks for which only one solution seems to be realizable (Szeri et al., 1983a).

The first systematic study of rotating disk flows, the subject of the present investigation, was made by Karman (1921). Karman postulated that axial velocity is independent of the radial coordinate. This postulate led to a similarity transformation, which was later shown by Batchelor (1951) to be applicable even when the fluid at infinity is rotating about the axis of the disk. Based on the examination of the governing equations, Batchelor showed that at high Reynolds numbers a thin boundary layer develops on each disk, with the main body of the fluid rotating at a constant rate, when the fluid is enclosed between two infinite disks. An excellent review of the work on infinite disk flows can be found in Zandbergen and Dijkstra (1987).

Finite disks have been studied by Szeri and Adams (1978), who used an approximation in which the radial variation of shear stress is neglected. The equations become parabolic in this approximation, and the flow is adequately described by a single dimensionless variable, the Ekman number, $E = \nu/s^2\omega$, where s represents the separation between the disks, ω is the rotational speed, and ν is the kinematic viscosity. When the film between the two finite disks is "thick" and either or both disks are rotating, Adams and Szeri (1982) find the flow to be characterized by five dimensionless parameters: the rotational Reynolds number $\mathrm{Re} = r_2\omega s/\nu$, the through-flow Reynolds number $R_Q = Q/2\pi\nu s$ where Q is the volumetric flow rate, the ratio of rotational speeds ω_2/ω_1, and two geometric ratios $\lambda = r_2/s$ and $\Delta = r_2/(r_2 - r_1)$. Here r_1 and $r_2 > r_1$ are the inner and outer radius, respectively, of the disks.

Szeri et al. (1983b) use laser-Doppler measurement of the velocities and find the equilibrium flow unique. With one disk rotating and the other stationary, the midradius "limiting flow" mimics the Batchelor profile of infinite disk theory. Other profiles, predicted by infinite disk theory to co-exist with the Batchelor profile, were neither observed experimentally nor calculated numerically by the finite disk solutions.

The flow between two finite rotating disks enclosed by a cylinder was investigated both numerically and experimentally by Dijkstra and van Heijst (1983). They also found the solution to be unique for all values of the parameters considered: of the Batchelor type for weak and of the Stewartson type for strong counterrotation.

More recently Brady and Durlofsky (1987) investigated the relationship of the axisymmetric flow between large but finite coaxial rotating disks to the Karman similarity solution. They combined asymptotics with numerical analysis in a method that has excellent potential for application to large aspect ratio problems in general, and showed that the finite disk solution and the similarity solution coincide over decreasing portion of the flow domain as the Reynolds number increases. Although this conclusion might seem counterintuitive and perhaps defies old wisdom, it does reinforce our assertion that finite disk and infinite disk flows are qualitatively different (Szeri et al., 1983b).

Some more recent work on finite disk flows includes Chang et al. (1989), Tzeng and Humphrey (1989), Fromm (1989), and Tzeng and Fromm (1990). These works are concerned with co-rotating disks, a problem that finds relevance in magnetic recording. A recent monograph by Owen and Rogers (1989) is also devoted to flow and heat transfer in rotating disk systems. While we are concerned with the flow and heat transfer in finite rotating disks with no superposed flow, most of Owen and Rogers' work considers superposed flow with radial or axial entry into and radial exit from the enclosure. This has applications in turbomachinery. More work on rotating cavities is by Randriamampianina et al. (1987, 1989). However, they consider

Address reprint requests to Professor Garg at his present address: NASA Lewis Research Center, Mail Stop 5-11, Cleveland, OH 44135, USA.

Received 30 March 1992; accepted 19 October 1992

mostly the flow and heat transfer in a Boussinesq fluid, using a spectral Tau–Chebyshev method.

Despite the availability of solutions for finite disks, the computation of disk flows is far from elementary. Our first goal in this paper is a comparison of two formulations: (1) the velocity formulation, and (2) the stream function formulation, both employing Galerkin's method with *B*-spline basis. Our second objective is to utilize the basic flow field in calculating heat transfer between the finite rotating disks for constant-property Newtonian fluid under various geometric and dynamic conditions. We will demonstrate, in comparison with our earlier experimental data, that either of the Galerkin-spline formulations leads to results of good accuracy.

2. Analysis

The flow field is bounded by two disks of radius r_2, located at $z = 0$ and $z = s$, in a cylindrical polar coordinate system (r, θ, z), and by two concentric cylinders of radii r_1 and r_2, $r_2 > r_1 > 0$. Figure 1 shows a part of the cylindrical cavity. The angular velocity of both the bottom disk and the outer cylinder, which is firmly attached to the bottom disk, is ω_1. The top disk and the inner cylinder are rotated with angular velocity ω_2.

Assuming rotational symmetry, the momentum and continuity equations take the form

$$u\frac{\partial u}{\partial r} - \frac{v^2}{r} + w\frac{\partial u}{\partial z} = \nu\left(\nabla^2 u - \frac{u}{r^2}\right) - \frac{1}{\rho}\frac{\partial p}{\partial r} \tag{1a}$$

$$\frac{u}{r}\frac{\partial}{\partial r}(rv) + w\frac{\partial v}{\partial z} = \nu\left(\nabla^2 v - \frac{v}{r^2}\right) \tag{1b}$$

$$u\frac{\partial w}{\partial r} + w\frac{\partial w}{\partial z} = \nu\nabla^2 w - \frac{1}{\rho}\frac{\partial p}{\partial z} \tag{1c}$$

$$\frac{\partial}{\partial r}(ru) + \frac{\partial}{\partial z}(rw) = 0 \tag{2}$$

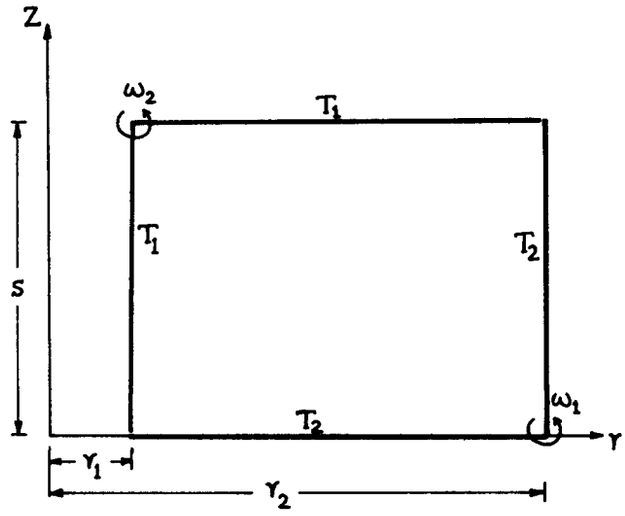

Figure 1 Part of the cylindrical cavity

Here (u, v, w) are the (r, θ, z) components of the velocity, p is the pressure, ρ is the fluid density, and ∇^2 is the Laplacian in cylindrical coordinates.

Since we intend to expand the unknowns in Equations 1 and 2 in series of splines, we normalize the coordinates (r, z) according to

$$x = \frac{r - r_1}{r_2 - r_1}, \quad y = \frac{z}{s}$$

so that

$$r = r_2 X(x),\ X = \frac{x}{\Delta} + \eta,\ \Delta = \frac{r_2}{r_2 - r_1},\ \eta = \frac{r_1}{r_2}$$

Notation

A_i, B_j	*B*-splines in x, y directions
C_m	Moment coefficient on one side of rotating disk (Equation 30a)
k	Thermal conductivity
L	Hydraulic diameter (Equation 24)
M	Frictional moment on one side of rotating disk (Equation 30b)
Nu	Nusselt number (Equation 24)
N_x, N_y	Dimension of approximating subspace (Equation 6)
p	Pressure
Pr	Prandtl number
q_i	Heat flux across the ith surface
r_1, r_2	Inner, outer radii of the cylinders
r, θ, z	Cylindrical coordinates
Re	Reynolds number $(=r_2\omega s/\nu)$
s	Axial separation between the disks
T	Temperature, normalized temperature $(=(T - T_1)/(T_2 - T_1))$
T_1	Temperature of inner cylinder and top disk
T_2	Temperature of outer cylinder and bottom disk
T_b	Bulk temperature, normalized bulk temperature (Equation 23)
X	Dimensionless radial coordinate $(=\eta + x/\Delta)$
u, v, w	Radial, tangential, and axial components of velocity, normalized velocity
x, y	Normalized radial and axial coordinates $(=(r - r_1)/(r_2 - r_1), z/s)$

Greek symbols

α	Thermal diffusivity
ε_q	Error in global energy conservation (Equation 22)
Δ	Geometric ratio $(= r_2/(r_2 - r_1))$
Γ	Geometric ratio $(= s/(r_2 - r_1))$
η	Geometric ratio $(= r_1/r_2)$
λ	Geometric ratio $(= r_2/s)$
ν	Kinematic viscosity
ρ	Density
Ψ	Dimensionless stream function (Equation 8)
ω	Maximum of ω_1, ω_2
ω_1	Angular velocity of bottom disk and outer cylinder
ω_2	Angular velocity of top disk and inner cylinder
Ω	Dimensionless angular velocity of fluid

2.1. Velocity formulation

The equations of motion and continuity are nondimensionalized according to

$$\{u, v, w\} = r_2\omega\left\{\bar{u}, X\Omega, \frac{\Delta}{\lambda}\bar{w}\right\}, \quad p = \rho r_2^2\omega^2\bar{p}$$

where we introduce the geometric parameter $\lambda = r_2/s$.

We eliminate the pressure by cross-differentiation between Equation 1a and 1c; this and nondimensionalization brings Equations 1 and 2 into the form:

$$\frac{\partial}{\partial y}\left[u\frac{\partial u}{\partial x} + w\frac{\partial u}{\partial y} - \frac{1}{\Delta}X\Omega^2\right] - \left(\frac{\Delta}{\lambda}\right)^2\frac{\partial}{\partial x}\left[u\frac{\partial w}{\partial x} + w\frac{\partial w}{\partial y}\right]$$
$$= \frac{1}{\Delta\lambda\,\mathrm{Re}}\left[\frac{\partial}{\partial y}\left(\nabla^2 u - \frac{u}{X^2}\right) - \left(\frac{\Delta}{\lambda}\right)^2\frac{\partial}{\partial x}(\nabla^2 w)\right] \tag{3a}$$

$$u\frac{\partial(X^2\Omega)}{\partial x} + w\frac{\partial(X^2\Omega)}{\partial y} = \frac{1}{\Delta\lambda\,\mathrm{Re}}[X\nabla^2(X\Omega) - \Omega] \tag{3b}$$

$$\frac{\partial(Xu)}{\partial x} + \frac{\partial(Xw)}{\partial y} = 0 \tag{4}$$

Here we have dropped the overscore bar for convenience, and the Laplacian is

$$\nabla^2 = \Delta^2\frac{\partial^2}{\partial x^2} + \frac{\Delta}{X}\frac{\partial}{\partial x} + \lambda^2\frac{\partial^2}{\partial y^2}$$

The only dynamic parameter of the problem is the Reynolds number, $\mathrm{Re} = r_2\omega s/\nu$.

The boundary conditions accompanying Equations 3 and 4 are

$$\begin{aligned} &u = 0; \quad v = X\omega_{1,2}; \quad w = 0 \quad \text{at} \quad y = 0, 1 \\ &u = 0; \quad v = \eta\omega_1, \omega_2; \quad w = 0 \quad \text{at} \quad x = 0, 1 \end{aligned} \tag{5a}$$

In addition to the boundary conditions, we also require satisfaction of the regularity conditions

$$\frac{\partial u}{\partial x} = 0 \quad \text{at} \quad x = 1 \quad \text{and} \quad \frac{\partial w}{\partial y} = 0 \quad \text{at} \quad y = 0 \tag{5b}$$

which are obtained by evaluating the continuity equation (Equation 4) on the boundaries. These additional conditions account for the increase in the order of the equations resulting from cross-differentiation (Galdi and Padula, 1989).

Let $\{A_i(x): 1 \le i \le N_x\}$ be the set of normalized B-splines relative to $\gamma_x, \beta_x, \delta_x$; and let $\{B_j(y): 1 \le j \le N_y\}$ be the set of normalized B-splines relative to $\gamma_y, \beta_y, \delta_y$ (de Boor, 1978). Here γ, β, and δ represent the order of the splines, the partition, and the smoothness index, respectively. We seek approximate solutions to Equations 3–5 in the form

$$\begin{aligned} u(x, y) &= \sum_{i=1}^{N_x}\sum_{j=1}^{N_y} u_{ij}A_i(x)B_j(y) \\ \Omega(x, y) &= \sum_{i=1}^{N_x}\sum_{j=1}^{N_y} \Omega_{ij}A_i(x)B_j(y) + \sum_{i=1}^{N_x}\sum_{j=1}^{N_y} f_i g_j A_i(x)B_j(y) \\ w(x, y) &= \sum_{i=1}^{N_x}\sum_{j=1}^{N_y} w_{ij}A_i(x)B_j(y) \end{aligned} \tag{6}$$

Here f_i, g_j are the spline-expansion coefficients of the functions $f(x) \in C^\infty[0, 1]$; $g(y) \in C^\infty[0, 1]$, which satisfy the boundary conditions (Equation 5). These functions are designed to smooth the boundary data and thus make the problem conform to the conditions of the Leray–Hopf–Ladyzhenskaya theorem on the existence of a solution of the Navier–Stokes equations in a finite domain (Benjamin and Mullin, 1981).

With the constraints

$$\begin{aligned} &u_{\alpha j} = \Omega_{\alpha j} = w_{\alpha j} = 0, \quad \alpha = 1, N_x, \quad u_{N_x-1,j} = 0, \quad \forall j \\ &u_{i\beta} = \Omega_{i\beta} = w_{i\beta} = 0, \quad \beta = 1, N_y, \quad w_{i2} = 0, \quad \forall i \end{aligned}$$

the expansions of Equation 6 satisfy all the boundary and regularity conditions of the problem. Denoting spline inner products by

$$\bar{Z}_{ijk}^{(\alpha)} = \int_0^1 B_i^{(a)}(z)B_j^{(b)}(z)B_k^{(c)}(z)dz, \quad \bar{z}_{ij}^{(\alpha)} = \int_0^1 B_i^{(b)}(z)B_j^{(c)}(z)dz$$

$$\overline{PK}_{ijk}^{(\alpha)} = \int_0^1 X^K(x)A_i^{(a)}(x)A_j^{(b)}(x)A_k^{(c)}(x)dx,$$

$$\overline{pK}_{ij}^{(\alpha)} = \int_0^1 X^K(x)A_i^{(b)}(x)A_j^{(c)}(x)dx$$

$$\overline{NL}_{ijk}^{(\alpha)} = \int_0^1 X^{-L}(x)A_i^{(a)}(x)A_j^{(b)}(x)A_k^{(c)}(x)dx,$$

$$\overline{nL}_{ij}^{(\alpha)} = \int_0^1 X^{-L}(x)A_i^{(b)}(x)A_j^{(c)}(x)dx$$

where $a \le b \le c$, $\alpha = a + b + c + 2$ (if $a > 0$) + 1 (if $b > 0$), $K \ge 0$, $L > 0$, the superscript a, b, or c denotes the ath, bth, or cth derivative of the B-spline. Projecting Equations 3 and 4 onto the subspace with basis $A_i \otimes B_j$, we derive the following set of nonlinear algebraic equations:

$$\begin{aligned} &\Delta\lambda\,\mathrm{Re}\sum_{i,m=1}^{N_x}\sum_{j,n=1}^{N_y}\left\{u_{mn}[u_{ij}\overline{P1}_{kim}^{(1)}\bar{Z}_{jnl}^{(1)} + w_{ij}\overline{P1}_{kim}^{(0)}\bar{Z}_{jln}^{(3)}]\right. \\ &\quad - \frac{1}{\Delta}(f_i f_m g_j g_n + 2f_i g_j\Omega_{mn} + \Omega_{ij}\Omega_{mn})\overline{P2}_{kim}^{(0)}\bar{Z}_{jnl}^{(1)} \\ &\quad - \left(\frac{\Delta}{\lambda}\right)^2 w_{mn}\left[u_{ij}\left(\frac{1}{\Delta}\overline{P0}_{kim}^{(1)} + \overline{P1}_{ikm}^{(3)}\right)\bar{Z}_{ljn}^{(0)}\right. \\ &\quad \left.\left. + w_{ij}\left(\frac{1}{\Delta}\overline{P0}_{kim}^{(0)} + \overline{P1}_{imk}^{(1)}\right)\bar{Z}_{ljn}^{(1)}\right]\right\} \\ &\quad + \sum_{i=1}^{N_x}\sum_{j=1}^{N_y}\left\{u_{ij}[\bar{z}_{lj}^{(1)}(\Delta^2\overline{p1}_{ki}^{(2)} + \Delta\overline{p0}_{ki}^{(1)} - \overline{n1}_{ki}^{(0)}) + \lambda^2\overline{p1}_{ki}^{(0)}\bar{z}_{lj}^{(4)}]\right. \\ &\quad \left. + \left(\frac{\Delta}{\lambda}\right)^2 w_{ij}[\bar{z}_{lj}^{(0)}(\Delta^2\overline{p1}_{ki}^{(4)} + \overline{n1}_{ki}^{(1)}) - \lambda^2\overline{p1}_{ki}^{(1)}\bar{z}_{lj}^{(2)}]\right\} = 0 \end{aligned} \tag{7a}$$

$$\begin{aligned} &\Delta\lambda\,\mathrm{Re}\sum_{i,m=1}^{N_x}\sum_{j,n=1}^{N_y}(f_m g_n + \Omega_{mn}) \\ &\quad \times\left[u_{ij}\bar{Z}_{ljn}^{(0)}\left(\frac{2}{\Delta}\overline{P2}_{kim}^{(0)} + \overline{P3}_{kim}^{(1)}\right) + w_{ij}\overline{P3}_{kim}^{(0)}\bar{Z}_{ljn}^{(1)}\right] \\ &\quad - \sum_{i=1}^{N_x}\sum_{j=1}^{N_y}(f_i g_j + \Omega_{ij})[\bar{z}_{ij}^{(0)}(\Delta^2\overline{p3}_{ki}^{(2)} + 3\Delta\overline{p2}_{ki}^{(1)}) \\ &\quad + \lambda^2\overline{p3}_{ki}^{(0)}\bar{z}_{ij}^{(2)}] = 0 \end{aligned} \tag{7b}$$

$$\sum_{i=1}^{N_x}\sum_{j=1}^{N_y}\left\{u_{ij}\bar{z}_{ij}^{(0)}\left(\frac{1}{\Delta}\overline{p1}_{ki}^{(0)} + \overline{p2}_{ik}^{(1)}\right) + w_{ij}\overline{p2}_{ki}^{(0)}\bar{z}_{jl}^{(1)}\right\} = 0 \tag{7c}$$

$$2 \le k \le N_x - 1, \quad 2 \le l \le N_y - 1$$

2.2. Stream function formulation

The equation of continuity (Equation 4) is identically satisfied by taking

$$\bar{u} = \frac{1}{X}\frac{\partial \bar{\Psi}}{\partial y}, \quad \bar{w} = -\frac{1}{X}\frac{\partial \bar{\Psi}}{\partial x} \tag{8}$$

where $\bar{\Psi}$ is the nondimensional stream function. We drop the overscore bar again.

Substituting Equation 8 into Equation 3, we find (Szeri et al., 1983b) that the equations of motion reduce to

$$\Delta \frac{\partial(\Psi, D^2\Psi)}{\partial(x, y)} + \lambda^2 \frac{\partial(X\Omega^2)}{\partial y} = -\frac{1}{\lambda \,\mathrm{Re}}\left(X^3 D^2 + 4\Delta \frac{\partial}{\partial x}\right) D^2\Psi \tag{9a}$$

$$\Delta \frac{\partial(\Psi, X^2\Omega)}{\partial(x, y)} = -\frac{1}{\lambda \,\mathrm{Re}} X^3 D^2(X^2\Omega) \tag{9b}$$

The operator D^2 in Equations 9a and 9b is defined by

$$D^2 = \frac{1}{X^2}\left(\Delta^2 \frac{\partial^2}{\partial x^2} - \frac{\Delta}{X}\frac{\partial}{\partial x} + \lambda^2 \frac{\partial^2}{\partial y^2}\right)$$

The boundary conditions for Equations 9a and 9b are

$$\frac{\partial \Psi}{\partial y} = \Psi = 0, \quad \Omega = \frac{\omega_1}{\omega}, \frac{\omega_2}{\omega} \quad \text{at} \quad y = 0, 1$$

$$\frac{\partial \Psi}{\partial x} = \Psi = 0, \quad \Omega = \eta \frac{\omega_2}{\omega}, \frac{\omega_1}{\omega} \quad \text{at} \quad x = 0, 1 \tag{10}$$

where $\omega = \max\{\omega_1, \omega_2\}$. We note that these conditions specify unbounded dissipation at points (0, 1) and (1, 1). This grossly unrealistic property is removed by smoothing out boundary data, as before.

We seek weak solutions of Equation 9 in the form

$$\Psi(x, y) = \sum_{i=3}^{N_x-2}\sum_{j=3}^{N_y-2} \Psi_{ij} A_i(x) B_j(y)$$

$$\Omega(x, y) = \sum_{s=3}^{N_x}\sum_{r=3}^{N_y} f_s g_r A_s(x) B_r(y) + \sum_{i=2}^{N_x-1}\sum_{j=2}^{N_y-1} \Omega_{ij} A_i(x) B_j(y) \tag{11}$$

Here f_s, $1 \le s \le N_x$; g_r, $1 \le r \le N_y$, are chosen such that Equation 11 satisfies the boundary conditions of the problem, leading to

$$f_1 = 0, \quad f_i = 1, \quad 2 \le i \le N_x$$
$$g_j = 1, \quad 1 \le j \le N_y - 1, \quad g_{N_y} = 0 \tag{12}$$

Galerkin's method with Equation 11 discretizes Equations 9a and 9b as follows:

$$\begin{aligned}
&\mathrm{Re}\sum_{i,p=3}^{N_x-2}\sum_{j,t=3}^{N_y-2} \Psi_{ij}\Psi_{pt}\{\bar{Z}^{(1)}_{ltj}[\Delta^2(\overline{N2}^{(2)}_{kip} - \overline{N2}^{(3)}_{ikp}) \\
&\quad + \Delta^3 \overline{N1}^{(4)}_{ikp} - \Delta \overline{N3}^{(1)}_{kip}] \\
&\quad + \lambda^2 \bar{Z}^{(4)}_{ljt}(\overline{N2}^{(0)}_{ipk} + \overline{N1}^{(1)}_{ipk}) + \bar{Z}^{(1)}_{jtl}(\Delta^2 \overline{N2}^{(3)}_{kip} - \Delta^3 \overline{N1}^{(4)}_{kip}) \\
&\quad - \lambda^2 \Delta \bar{Z}^{(4)}_{jlt} \overline{N1}^{(1)}_{kpi}\} \\
&\quad + 2\lambda\,\mathrm{Re}\left[\sum_{s=2}^{N_x}\sum_{r=1}^{N_y-1}\sum_{p=2}^{N_x-1}\sum_{t=2}^{N_y-1} f_s g_r \Omega_{pt} \overline{P2}^{(0)}_{spk}(\bar{Z}^{(1)}_{rlt} + \bar{Z}^{(1)}_{tlr}) \right. \\
&\quad + \sum_{i,p=2}^{N_x-1}\sum_{j,t=2}^{N_y-1} \Omega_{ij}\Omega_{pt} \overline{P2}^{(0)}_{ipk} \bar{Z}^{(1)}_{ljt} \\
&\quad \left. + \sum_{s,p=2}^{N_x}\sum_{r,t=1}^{N_y-1} f_s g_r f_p g_t \overline{P2}^{(0)}_{spk} \bar{Z}^{(1)}_{rlt}\right]
\end{aligned}$$

$$\begin{aligned}
&+ \sum_{i=3}^{N_x-2}\sum_{j=3}^{N_y-2} \Psi_{ij}[\bar{z}^{(0)}_{lj}(\Delta^4 \overline{p0}^{(5)}_{ki} + 2\Delta^3 \overline{n1}^{(4)}_{ki} \\
&\quad + \Delta^2 \overline{n2}^{(2)}_{ki} - 3\Delta \overline{n3}^{(1)}_{ki}) \\
&\quad + 2\Delta\lambda^2 \bar{z}^{(2)}_{lj}(\Delta \overline{p0}^{(2)}_{ki} - \overline{n1}^{(1)}_{ki}) + \lambda^4 \bar{z}^{(5)}_{lj} \overline{p0}^{(0)}_{ki}] = 0
\end{aligned} \tag{13a}$$

$$\begin{aligned}
&\mathrm{Re}\sum_{i=3}^{N_x-2}\sum_{j=3}^{N_y-2}\sum_{p=2}^{N_x-1}\sum_{t=2}^{N_y-1} \Psi_{ij}\Omega_{pt} \\
&\quad \times [\bar{Z}^{(1)}_{ltj}(2\overline{P2}^{(0)}_{kip} + \Delta \overline{P3}^{(1)}_{kip}) - \Delta \overline{P3}^{(1)}_{kpi} \bar{Z}^{(1)}_{ljt}] \\
&\quad - \sum_{p=2}^{N_x-1}\sum_{t=2}^{N_y-1} \Omega_{pt}[\bar{z}^{(0)}_{lt}(3\Delta \overline{p3}^{(1)}_{kp} + \Delta^2 \overline{p4}^{(2)}_{kp}) + \lambda^2 \overline{p4}^{(0)}_{kp} \bar{z}^{(2)}_{lt}] \\
&\quad + \mathrm{Re}\sum_{i=3}^{N_x-2}\sum_{j=3}^{N_y-2}\sum_{s=2}^{N_x}\sum_{r=1}^{N_y-1} \Psi_{ij} f_s g_r \\
&\quad \times [\bar{Z}^{(1)}_{rlj}(2\overline{P2}^{(0)}_{kis} + \Delta \overline{P3}^{(1)}_{kis}) - \Delta \bar{Z}^{(1)}_{ljr} \overline{P3}^{(1)}_{ksi}] \\
&\quad - \sum_{s=2}^{N_x}\sum_{r=1}^{N_y-1} f_s g_r[\Delta \bar{z}^{(0)}_{rl}(3\overline{p3}^{(1)}_{ks} + \Delta \overline{p4}^{(2)}_{ks}) + \lambda \bar{z}^{(2)}_{lr} \overline{p4}^{(0)}_{ks}] = 0
\end{aligned} \tag{13b}$$

We note here that although Equation 9a is fourth order in Ψ, we require only that A_i, $B_j \in C^2$ (0, 1), on account of integration by parts when carrying out the discretization. It is this that permits us to employ the stream function formulation. This technique is, of course, not available when employing finite differences, which forces one to solve a stream function-vorticity formulation.

2.3. Equation of energy

The nondimensional form of the energy equation is

$$\mathrm{Re}\left[\bar{u}\frac{\partial \bar{T}}{\partial x} + \bar{w}\frac{\partial \bar{T}}{\partial y}\right] = \frac{\Delta}{\lambda \,\mathrm{Pr}}\left[\frac{1}{X}\frac{\partial}{\partial x}\left(X\frac{\partial \bar{T}}{\partial x}\right) + \left(\frac{\lambda}{\Delta}\right)^2 \frac{\partial^2 \bar{T}}{\partial y^2}\right] \tag{14}$$

and we adopt the boundary conditions

$$\bar{T}(0, y) = 0, \quad \bar{T}(1, y) = 1, \quad \bar{T}(x, 0) = 1, \; \bar{T}(x, 1) = 0 \tag{15}$$

Here $\bar{T} = (T - T_1)/(T_2 - T_1)$ is the nondimensional temperature, and $\mathrm{Pr} = \nu/\alpha$ is the Prandtl number. We again drop the overscore bar.

Provided that

$$h_1 = 0, \quad h_i = 1, \quad 2 \le i \le N_x$$
$$k_j = 1, \quad 1 \le j \le N_y - 1, \quad k_{N_y} = 0 \tag{16}$$

the expansion

$$T(x, y) = \sum_{i=2}^{N_x-1}\sum_{j=2}^{N_y-1} T_{ij} A_i(x) B_j(y) + \sum_{i=1}^{N_x}\sum_{j=1}^{N_y} h_i k_j A_i(x) B_j(y) \tag{17}$$

satisfies the thermal boundary conditions (Equation 15). It will also satisfy the energy equation (Equation 14), provided that the T_{ij} solve the linear system

$$\sum_{i=2}^{N_x-1}\sum_{j=2}^{N_y-1} A_{klij} T_{ij} = -\sum_{i=1}^{N_x}\sum_{j=1}^{N_y} A_{klij} h_i k_j \tag{18}$$

where

$$\begin{aligned}
A_{klij} = &\frac{\Delta}{\lambda \,\mathrm{Pr}}\left[\bar{z}^{(0)}_{lj}\left(\overline{p1}^{(2)}_{ki} + \frac{1}{\Delta}\overline{p0}^{(1)}_{ki}\right) + \left(\frac{\lambda}{\Delta}\right)^2 \overline{p1}^{(0)}_{ki} \bar{z}^{(2)}_{lj}\right] \\
&- \mathrm{Re}\sum_{m=1}^{N_x}\sum_{n=1}^{N_y}[u_{mn} \overline{P1}^{(1)}_{kmi} \bar{Z}^{(0)}_{lnj} + w_{mn} \overline{P1}^{(0)}_{klm} \bar{Z}^{(1)}_{lnj}]
\end{aligned} \tag{19}$$

and u_{mn}, w_{mn} are from Equations 7 or 8.

Let q_i, $1 \le i \le 4$, denote the heat flux into the fluid across the ith surface of the enclosure, and let $\bar{q}_i$ be its nondimensional counterpart. We then write

$$\bar{q}_i = \frac{q_i}{2\pi k s(T_2 - T_1)}, \quad 1 \le i \le 4 \tag{20}$$

Here $i = 1, 2, 3$, and 4 refers to the surfaces $x = 0$, $y = 0$, $x = 1$, and $y = 1$, respectively.

Employing the notation

$$\bar{a}_i = \int_0^1 X(x)A_i(x)dx, \quad \bar{b}_j = \int_0^1 B_j(y)dy$$

we find

$$\bar{q}_1 = \eta\Delta A_1'(0)\left\{\sum_{j=2}^{N_y-1} T_{2,j}\bar{b}_j + \sum_{j=1}^{N_y} k_j\bar{b}_j\right\}$$

$$\bar{q}_2 = \frac{\lambda^2 B_1'(0)}{\Delta}\sum_{i=2}^{N_x-1} \bar{a}_i T_{i,2}$$

$$\bar{q}_3 = -\eta\Delta A_{N_x}'(1)\sum_{j=2}^{N_y-1} T_{N_x-1,j}\bar{b}_j$$

$$\bar{q}_4 = -\frac{\lambda^2 B_{N_y}'(1)}{\Delta}\left\{\sum_{i=2}^{N_x-1} \bar{a}_i T_{i,N_y-1} + \sum_{i=1}^{N_x} \bar{a}_i h_i\right\} \tag{21}$$

Global energy conservation leads to the equation $\sum_{i=1}^{4} \bar{q}_i = 0$. In order to judge the accuracy of our numerical scheme for calculating the temperature distribution $T(r, z)$, we compute an error ε_q with definition

$$\varepsilon_q = \frac{|\bar{q}_1 + \bar{q}_2 + \bar{q}_3 + \bar{q}_4|}{|\bar{q}_1| + |\bar{q}_2| + |\bar{q}_3| + |\bar{q}_4|} \tag{22}$$

As the flow under consideration forms a closed system, we define the Nusselt number with reference to the bulk temperature, T_b, which is defined as

$$T_b = \frac{\int_{r_1}^{r_2}\int_0^s vT\,dr\,dz}{\int_{r_1}^{r_2}\int_0^s v\,dr\,dz} \tag{23a}$$

or, in nondimensional form, as

$$\bar{T}_b = \frac{\sum_{i=1}^{N_x}\sum_{j=1}^{N_y}(T_{ij} + h_i k_j)(\Omega_{ij} + f_i g_j)\bar{a}_i\bar{b}_j}{\sum_{i=1}^{N_x}\sum_{j=1}^{N_y}(\Omega_{ij} + f_i g_j)\bar{a}_i\bar{b}_j} \tag{23b}$$

The Nusselt numbers $\mathrm{Nu}^{(i)}$, $i = 1, 2, 3, 4$, are now defined in terms of the heat-flow rates q_i, $i = 1, 2, 3, 4$, and the bulk temperature as follows (dropping the overscore bar again):

$$q_1 = -\mathrm{Nu}^{(1)}\left(\frac{k}{L}\right)2\pi r_1 s T_b \tag{24a}$$

$$q_2 = \mathrm{Nu}^{(2)}\left(\frac{k}{L}\right)\pi(r_2^2 - r_1^2)(1 - T_b) \tag{24b}$$

$$q_3 = \mathrm{Nu}^{(3)}\left(\frac{k}{L}\right)2\pi r_2 s(1 - T_b) \tag{24c}$$

$$q_4 = -\mathrm{Nu}^{(4)}\left(\frac{k}{L}\right)\pi(r_2^2 - r_1^2)T_b \tag{24d}$$

Here $L = 2s/(1 + \Gamma)$ is the hydraulic diameter of the annulus, and $\Gamma = s/(r_2 - r_1)$.

2.4. Solution of the Nonlinear equations

The non-linear equations (either Equation 7 or 13) take the form

$$G(\xi, \phi) = 0 \tag{25}$$

where G: $R^n = \Xi \oplus \Phi \to R^m$ is a C^l-mapping ($l > 2$), $\dim \Xi = m$ and $\dim \Phi = n - m > 1$. Here $\xi \in \Xi$ is a vector of state variables and $\phi \in \Phi$ a vector of parameters λ, Δ, Re, Pr.

The solution set of Equation 24 is a τ-dimensional manifold in R^n. When $\tau = 1$ the manifold becomes a path. We intend to use the Gauss–Newton method for local iteration, and the method of continuation for tracing the path. For convenience we shall use ζ instead of (ξ, ϕ) in the sequel.

2.4.1. Local iteration. Let ζ^k be our current point. The next point ζ^{k+1} of the iteration sequence is defined by the Gauss–Newton method as follows (Ortega and Rheinboldt, 1970):

$$\zeta^{k+1} = \zeta^k - [DG(\zeta^k)^T DG(\zeta^k)^{-1}]DG(\zeta^k)^T G(\zeta^k) \tag{26a}$$

where $DG(\zeta^k)$ is the Jacobian of G evaluated at ζ^k. Equation 26a is inconvenient computationally. It can be verified, however, that ζ^{k+1} will satisfy Equation 26a if it satisfies the condition

$$DG(\zeta^k)(\zeta^k - \zeta^{k+1}) = G(\zeta^k) \tag{26b}$$

Numerically, Equation 26b can be implemented in various ways. With QR-factorization of $DG(\zeta^k)^T$, we have

$$\zeta^k - \zeta^{k+1} = Q\begin{pmatrix} R^{-T} \\ 0 \end{pmatrix}G(\zeta^k) \tag{27}$$

Then starting from any point ζ sufficiently close to the solution manifold, we apply the following algorithm:

(i) set $\zeta^0 = \zeta$;
(ii) for $k = 0, 1, \ldots$ until convergence
  (a) solve $R^T\mu = G(\zeta^k)$ for $\mu \in R^m$;
  (b) compute the next iterate $\zeta^{k+1} = \zeta^k - Q\begin{pmatrix}\mu \\ 0\end{pmatrix}$

2.4.2. Continuation along the path. For a solution point ζ on the path, we consider again the QR-factorization of $DG(\zeta)^T$:

$$DG(\zeta)^T = Q\begin{pmatrix} R \\ 0 \end{pmatrix} \tag{28}$$

Clearly the last column vector of the orthogonal matrix Q, namely Qe_n, is the tangent vector of the path. Here $e_n = (0, \ldots, 0, 1)^T \in R^n$ at ζ.

The simplest way to get a predictor for the next point on the path is to set

$$\zeta^0 = \zeta + \sigma Qe_n \tag{29}$$

where σ is a suitable step size. The direction of the continuation can be controlled by the sign of the last component of Qe_n.

Continuation is necessary at high Reynolds numbers in order to achieve convergence, when $\zeta^0 = 0$ is not in the neighborhood of attraction of the solution. But even at low Reynolds numbers the computational effort required is decreased when using path continuation.

3. Results and discussion

We set as our first task a comparison of the two formulations for velocity field. Let $\hat{n}$ and n represent the size of the nonlinear algebraic system for the primitive variable formulation (Equation 6) and the stream function formulation (Equation 11), respectively. By assigning $N = N_x = N_y$, we have $\hat{n} = (N - 2)(3N - 8)$ and $n = (N - 4)^2 + (N - 2)^2$. For the sequence $N = \{15, 20, 25, 31\}$ we obtain $\hat{n} = \{481, 936, 1541, 2465\}$ and $n = \{290, 580, 970, 1570\}$. In Tables 1 and 2 we show

Table 1 Azimuthal velocity ($\Delta = 1.0714$, $\lambda = 20.16$, Re = 1054.51, $x = 0.4$): (a) stream function formulation; (b) velocity formulation

y	Formulation	$N = 15$	$N = 20$	$N = 25$	$N = 31$
0.2	(a)	0.20274	0.20156	0.20070	0.20021
	(b)	—	0.19316	0.19797	0.19853
0.4	(a)	0.14368	0.14335	0.14288	0.14245
	(b)	—	0.13410	0.14338	0.14232
0.6	(a)	0.12094	0.12085	0.12054	0.12052
	(b)	—	0.11092	0.12285	0.12052
0.8	(a)	0.07166	0.07144	0.07130	0.07129
	(b)	—	0.06463	0.07328	0.07147

Table 2 Radial velocity ($\Delta = 1.0714$, $\lambda = 20.16$, Re = 1054.51, $x = 0.4$): (a) stream function formulation; (b) velocity formulation

y	Formulation	$N = 15$	$N = 20$	$N = 25$	$N = 31$
0.2	(a)	0.06464	0.06393	0.06376	0.06372
	(b)	—	0.05680	0.06433	0.06437
0.4	(a)	0.00322	0.00332	0.00339	0.00341
	(b)	—	0.00106	0.00392	0.00376
0.6	(a)	−0.03771	−0.03778	−0.03764	−0.03766
	(b)	—	−0.03468	−0.03758	−0.03742
0.8	(a)	−0.04679	−0.04649	−0.04641	−0.04639
	(b)	—	−0.04080	−0.04704	−0.04625

results of some numerical experiments. Increasing N in steps and calculating azimuthal velocity (Table 1) and radial velocity (Table 2) from the two formulations, we have rapid convergence with N increasing. But while the stream function results already seem to be accurate at $N = 20$, the velocity formulation yields comparable accuracy only with $N = 31$ in some cases. This lends unquestionable superiority to the stream function formulation for the present problem. This is also our conclusion from a study on natural convection in a horizontal cylindrical annulus (Garg and Szeri, 1992). We are thus advocating the stream function formulation when employing Galerkin's method, for the axisymmetric flow of a Newtonian fluid.

By comparison with experimental data we can also demonstrate that the convergence of the numerical solution is to the true solution. Here we compare with the experimental data of Szeri et al. (1983b). This data was obtained by laser-Doppler measurements in an apparatus of $r_2 = 0.254$ m, $r_1 = 0.0126$ m, and $s = 0.0126$ m. Figure 2 depicts azimuthal velocity at five radial locations, $x = 0.1, 0.3, 0.5, 0.7, 0.9$, while Figure 3 shows radial velocity at two locations, $x = 0.5, 0.7$. Only the bottom disk and outer cylinder are rotated in this experiment, and calculations were performed with $N_x = N_y = 31$, using the stream function formulation. $N_x = N_y = 31$ was the maximum size the University of Pittsburgh's VAX, the computer used in our initial computations, could handle. Figure 4 shows the radial velocity for half channel at four different locations in a thin, $\lambda = 80$, film. Agreement with experiments is, again, acceptable. Numerical prediction and experimental data are compared next for flow between counterrotating disks. Figure 5 shows results for azimuthal velocity, indicating good agreement with experimental data. Comparison for radial velocities, shown in Figure 6, is less satisfactory. The reason for better results on azimuthal velocity than on radial velocity is, of course, that while the former is induced by the motion of the boundaries, the latter is brought about by the pressure field.

Figure 7 compares the moment coefficient, C_m, on one side of the rotating disk for the present results against those

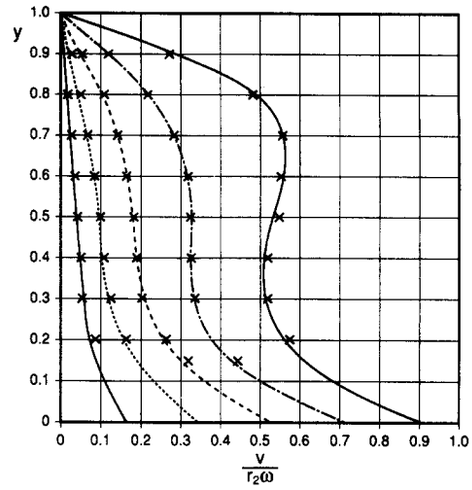

Figure 2 Azimuthal velocity, $\Delta = 1.0714$, $\lambda = 20.16$, Re = 997, $\omega_2/\omega_1 = 0$ (Theory: ———, $x = 0.9$; —·—, $x = 0.7$; ----, $x = 0.5$; . . . , $x = 0.3$; ———, $x = 0.1$. Experiment: ×)

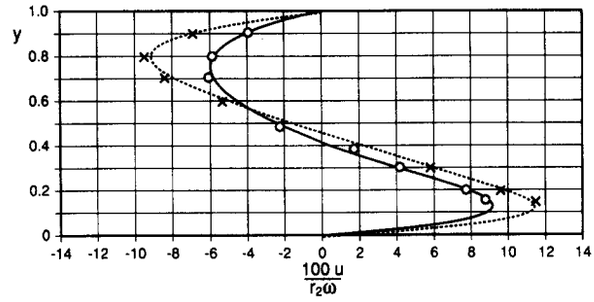

Figure 3 Radial velocity, $\Delta = 1.0714$, $\lambda = 20.16$, Re = 997, $\omega_2/\omega_1 = 0$ (Theory: ———, $x = 0.5$; ----, $x = 0.7$. Experiment: ○, $x = 0.5$; ×, $x = 0.7$)

obtained by (1) Randriamampianina et al. (1989) using the spectral Tau–Chebyshev method, (2) Daily and Nece (1960) based on a theoretical analysis, and (3) Vaughan (1986) using a finite-difference method. Clearly the agreement between all four different techniques is very good. The moment coefficient

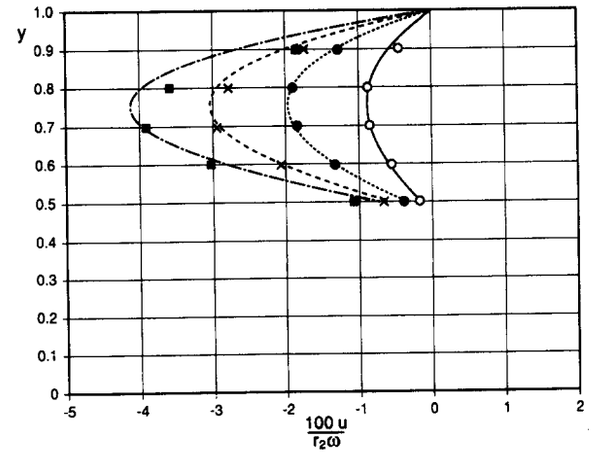

Figure 4 Radial velocity, $\Delta = 1.0714$, $\lambda = 80.0$, Re = 670, $\omega_2/\omega_1 = 0$ (Theory: ———, $x = 0.1$; . . . , $x = 0.3$; ----, $x = 0.5$; —·—, $x = 0.7$. Experiment: ○, $x = 0.1$; ●, $x = 0.3$; ×, $x = 0.5$; ■, $x = 0.7$)

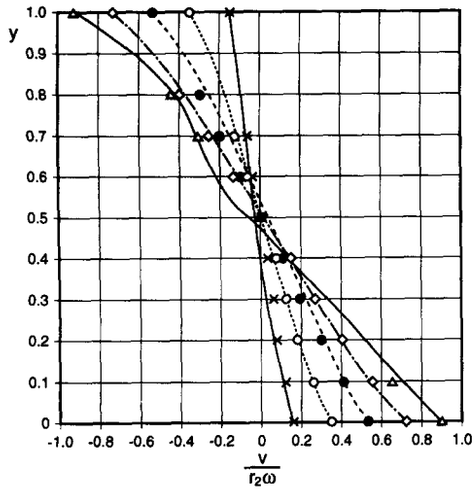

Figure 5 Azimuthal velocity, $\Delta = 1.0714$, $\lambda = 20.16$, Re = 499, $\omega_2/\omega_1 = -0.977$ (Theory: ———, $x = 0.1$; . . . , $x = 0.3$; ----, $x = 0.5$; —·—, $x = 0.7$; ———, $x = 0.9$. Experiment: ×, $x = 0.1$; ○, $x = 0.3$; ●, $x = 0.5$; ◇, $x = 0.7$; Δ, $x = 0.9$)

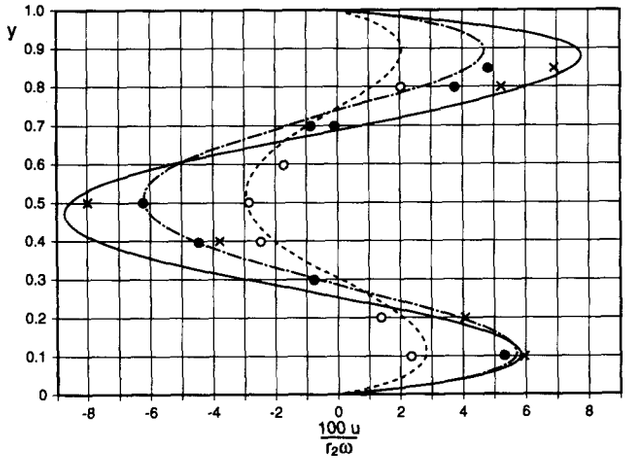

Figure 6 Radial velocity, $\Delta = 1.0714$, $\lambda = 20.16$, Re = 499, $\omega_2/\omega_1 = -0.977$ (Theory: ----, $x = 0.3$; —·—, $x = 0.7$; ———, $x = 0.9$. Experiment: ○, $x = 0.3$; ●, $x = 0.7$; ×, $x = 0.9$)

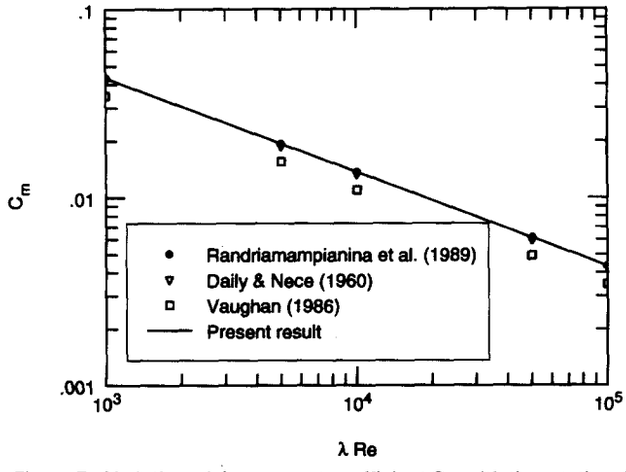

Figure 7 Variation of the moment coefficient C_m with the rotational Reynolds number λRe: Comparison between different solution techniques

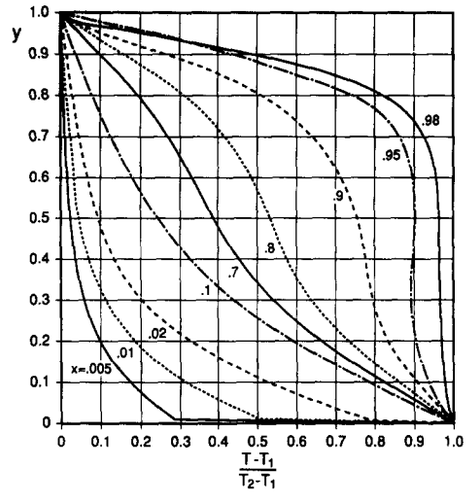

Figure 8 Temperature profiles at various x locations, $\Delta = 1.0714$, $\lambda = 20.16$, Re = 997, $\omega_2/\omega_1 = 0$, Pr = 0.7

is given by

$$C_m = \frac{2M}{\rho\omega^2 r_2^5} \tag{30a}$$

where the frictional moment, M, is given by

$$M = \int_{r_1}^{r_2} 2\pi r^2 \rho\nu\left(\frac{\partial u}{\partial z} + \frac{\partial w}{\partial r}\right)\Big|_{z=0} dr \tag{30b}$$

In Equations 30, all quantities except C_m are dimensional.

Having demonstrated the accuracy of the velocity field calculations, we now turn attention to heat transfer between the rotating disks. Figures 8 and 9 display temperature profiles in a "thick" film, $s = 0.0126$ m, ($\lambda = 20.16$), and in a "thin" film, $s = 0.003175$ m, ($\lambda = 80$), respectively. Close to the inner cylinder, $x < 0.1$, these figures display discontinuity of $\partial T/\partial y$ near the bottom disk. This aphysical situation arises in the computation due to the presence of a singularity in the thermal boundary conditions at the point $(x, y) = (0, 0)$. There is another singularity in temperature boundary data at $(x, y) = (1, 1)$ leading to a similar, but not shown, discontinuity in $\partial T/\partial y$.

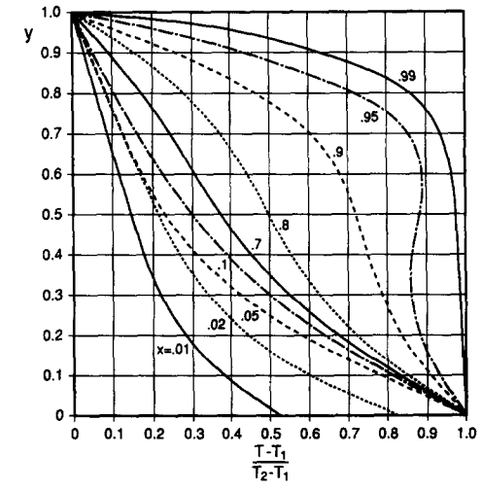

Figure 9 Temperature profiles at various x locations, $\Delta = 1.0714$, $\lambda = 80.0$, Re = 3369, $\omega_2/\omega_1 = 0$, Pr = 0.7

Table 3 Error ε_q in satisfying global energy conservation

λ	Re	ε_q
20.16	203	0.061
	402	0.045
	600	0.035
	799	0.029
	997	0.025
80.0	45	0.032
	545	0.030
	1210	0.025
	2289	0.019
	3370	0.016

To check global energy conservation, we computed the error, ε_q, of Equation 22. Table 3 shows results of the computer experiment. In these calculations, heat transfer rates, q_i, $i = 1, 2, 3, 4$, were evaluated not strictly on the boundary but at $x = 0.005$, $y = 0.005$, $x = 0.995$, $y = 0.995$, respectively. This was necessary because of the singularities in the temperature boundary data.

It is significant to note here that global energy conservation improves with increasing Reynolds number in our computational scheme. This counterintuitive result is due to the fact that the inner and outer cylinders lose importance for heat transfer, that is, more and more of the action is concentrated at the disks, as the Reynolds number is increased. In consequence, the singularities in the boundary data also lose significance with increasing Reynolds number.

The Nusselt number is plotted against Reynolds number in Figures 10 to 12. Figure 10 displays conditions for "thin" film geometry, $\lambda = 80$, with one disk held stationary. The Nusselt numbers are constant for Re < 200. For Re > 1000, heat transferred from or to the cylinders becomes less significant, and most of the heat transfer occurs between the two disks. The shrouds are important for Re > 1000 only in defining the flow field but not the heat transfer. Figure 11 displays Nu versus Re for a "thick" film, $\lambda = 20.16$. Qualitatively there is little change in comparison with the previous case for the Nusselt number on the disks, but the Nusselt number on both the cylinders behaves differently. A greater role for heat transferred from or to the shrouds is seen for this case than that for the "thin" film case of Figure 10.

For counterrotating cylinders, Figure 12, the Nusselt number varies little with the Reynolds number for Re < 200 on all the surfaces. Besides, the Nusselt number values in this case are about an order of magnitude smaller than those in Figures 10 and 11.

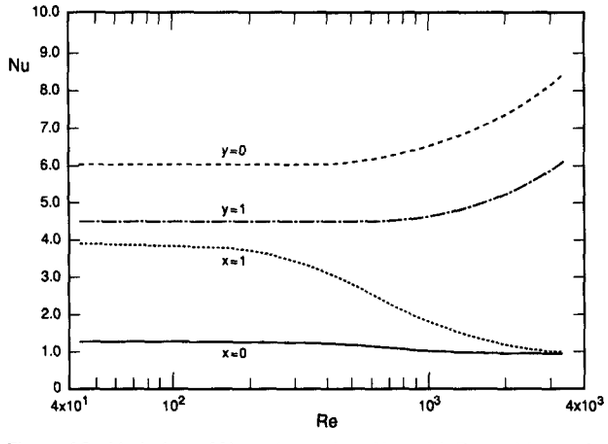

Figure 10 Variation of Nusselt number, Nu, with Reynolds number, Re. $\Delta = 1.0714$, $\lambda = 80.0$, $\omega_2/\omega_1 = 0$, Pr = 0.7

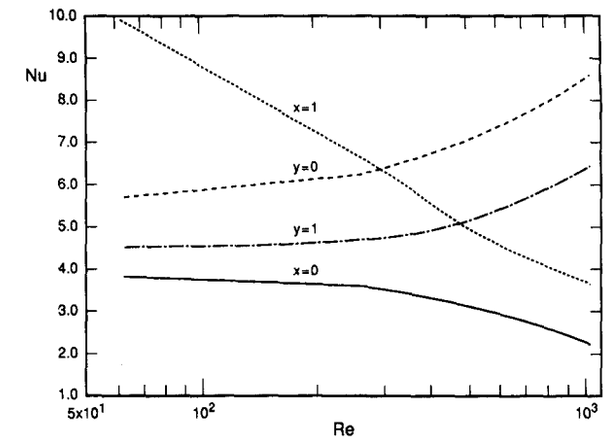

Figure 11 Variation of Nusselt number, Nu, with Reynolds number, Re. $\Delta = 1.0714$, $\lambda = 20.16$, $\omega_2/\omega_1 = 0$, Pr = 0.7

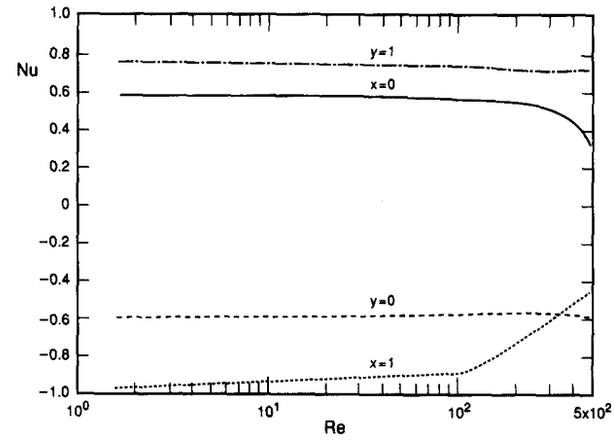

Figure 12 Variation of Nusselt number, Nu, with Reynolds number, Re. $\Delta = 1.0714$, $\lambda = 20.16$, $\omega_2/\omega_1 = -0.975$, Pr = 0.7

Acknowledgment

A. Z. Szeri was partially supported by the National Science Foundation, under Grant No. CTS-8920956, during this project. Computations were made possible through a grant by the Pittsburgh Supercomputing Center for use of its CRAY Y-MP/832. Both these supports are gratefully acknowledged. The authors would also like to acknowledge the referees for their useful and stimulating comments.

References

Adams, M. L. and Szeri, A. Z. 1982. Incompressible flow between finite disks. *J. Appl. Mech.*, **49**, 1–9

Batchelor, G. K. 1951. Note on a class of solutions of the Navier–Stokes equations representing rotationally symmetric flow. *Q. J. Mech. Appl. Math.*, **4**, 29–41

Benjamin, T. B. 1978. Bifurcation phenomena in steady flows of a viscous fluid. I. Theory. *Proc. R. Soc. (Lond.)*, **A359**, 1–26

Benjamin, T. B. and Mullin, T. 1981. Anomalous modes in the Taylor experiment. *Proc. R. Soc. (Lond.)*, **377**, 221–249

Brady, J. F. and Durlofsky, L. 1987. On rotating disk flow. *J. Fluid Mech.*, **175**, 363–394

Chang, C. J., Schuler, C. A., Humphrey, J. A. C., and Greif, R. 1989. Flow and heat transfer in the space between two corotating disks in an axisymmetric enclosure. *J. Heat Transfer*, **111**, 625–632

Dai, R. X., and Szeri, A. Z. 1990. A numerical study of finite Taylor flows. *Int. J. Non-Linear Mech.*, **25**, 45–60

Daily, J. W., and Nece, R. E. 1960. Chamber dimension effects on induced flow and frictional resistance of enclosed rotating disks. *J. Basic Eng.*, **88**, 217–232

de Boor, C. 1978. *A Practical Guide to Splines.* Springer-Verlag, Berlin

Dijkstra, D., and van Heijst, G. J. F. 1983. The flow between two finite rotating disks enclosed by a cylinder. *J Fluid Mech.*, **128**, 123–154

Fromm, J. E. 1989. Direct calculation of turbulence in rotational fluid flows. IBM Research Rep. RJ6666

Galdi, G. P., and Padula, M. 1989. A new approach to energy theory in the stability of fluid motion. *Arch. Rat. Mech. Anal.*, **110**, 187–286

Garg, V. K., and Szeri, A. Z. 1992. Natural convection in a horizontal concentric cylindrical annulus. *Int. J. Numer. Meth. Heat Fluid Flow*, **2**, 455–467

von Karman, T. 1921. Uber laminare und turbulente reibung. *Z. Angew. Math. Mech.*, **1**, 233–252

Ortega, J. M., and Rheinboldt, W. C. 1970. *Iterative Solution of Non-Linear Equations in Several Variables.* Academic Press, San Diego

Owen, J. M., and Rogers, R. H. 1989. *Flow and Heat Transfer in Rotating-Disc Systems*, **1**, Research Studies Press, England

Randriamampianina, A., Bontoux, P., and Roux, B. 1987. Ecoulements induits par la force gravifique dans une cavite cylindrique en rotation. *Int. J. Heat Mass Transfer*, **30**, 1275–1292

Randriamampianina, A., Chaouche, A., Segura, E., and Bontoux, P. 1989. Numerical predictions for the flow and heat transfer in gas turbine cooling systems. *Proc. 5th Int. Symp. Numer. Meth. Eng.*, **2**, 525–531

Szeri, A. Z. and Adams, M. L. 1978. Laminar throughflow between closely spaced rotating disks. *J. Fluid Mech.*, **86**, 1–14

Szeri, A. Z., Giron, A., Schneider, S. J., and Kaufman, H. N. 1983a. Flow between rotating disks. Part 2. Stability. *J. Fluid Mech.*, **134**, 133–154

Szeri, A. Z., Schneider, S. J., Labbe, F., and Kaufman, H. N. 1983b. Flow between rotating disks. Part 1. Basic flow. *J. Fluid Mech.*, **134**, 103–131

Tzeng, H. M., and Humphrey, J. A. C. 1989. Corotating disk flow in an axisymmetric enclosure with and without a bluff body. *Proc. 7th Symp. Turbulent Shear Flows*, Stanford University Press, Stanford, CA

Tzeng, H. M., and Fromm, J. E. 1990. Air flow study in a cylindrical enclosure containing multiple corotating disks. *ISROMAC*-3, Hawaii

Vaughan, C. 1986. A numerical investigation into the effect of an external flow field on the sealing of a rotor-stator cavity. D. Phil. Thesis, University of Sussex, England

Zandbergen, P. J., and Dijkstra, D. 1987. Von Karman swirling flows. *Annu. Rev. Fluid Mech.*, **19**, 465–491